Green Chemistry

PAPER

View Article Online
View Journal | View Issue

Cite this: *Green Chem.*, 2023, **25**, 1417

Light-driven Pickering interfacial catalysis for the oxidation of alkenes at near-room temperature†

Yaoyao Feng,[a] Jean-François Dechezelles,[a] Quentin D'Acremont,[b] Emmanuel Courtade,[b] Vincent De Waele,[c] Marc Pera-Titus *[d] and Véronique Nardello-Rataj *[a]

Received 2nd December 2022,
Accepted 24th January 2023

DOI: 10.1039/d2gc04591e

rsc.li/greenchem

In this study, we have developed an emulsion system combining plasmonic Au-loaded amphiphilic silica nanoparticles (Au/SiO_2–C_3) and tri(dodecyltrimethylammonium) phosphotungstate ($[C_{12}]_3[PW_{12}O_{40}]$) nanoparticles acting as an on-site photoassisted heater/activator and a catalyst, respectively, at the water/oil interface. The system exhibits a 5-fold increase of activity compared to the thermal reaction for the near-room temperature oxidation of alkenes with H_2O_2. The nanoparticles show excellent recyclability and structural stability. This study opens an avenue to design multiphase photoreactors for oxidation reactions at mild temperature, with a potential energy saving of 74% compared to that of thermally heated reactors at isoconversion.

Introduction

Owing to localized surface plasmon resonance (LSPR), noble metal nanoparticles (NPs) can absorb light to generate hot electrons and cause local heating by hyperthermia.[1] These properties allow efficient light-to-energy conversion and energy transfer to the local microenvironment around the NPs. Among noble metals, Au NPs are most commonly used as plasmonic materials and catalysts due to their low reactivity, easy fabrication and facile application in targeted therapies driven by local heating.[2]

Depending on the decay pathways of plasmonic energy, the mechanisms of hot carriers in the chemical reaction are proposed as follows: (1) optically excited hot electrons can inject into the electron-accepting states of the nearby surface and can take part in the reaction, (2) photo-induced hot carriers play a negligible role in activating the adsorbed reactants, but convert energy into heat through energy exchange between electrons and phonons, and (3) both hot carrier-driven reactant activation and photothermal heating co-exist and can act synergistically to drive chemical reactions. The plasmonic properties of Au NPs are dictated by their size, shape (*e.g.*, nanospheres, nanorods, nanoshells, *etc.*) and composition, as well as by the surrounding conditions such as pH, concentration and ionic environment.[3]

Based on their LSPR properties, Au NPs have been used as plasmonic/photothermal catalysts or catalyst components for a variety of reactions,[4] including peroxide decomposition,[5] oxidation,[6] oxidation/amidation,[7] reduction,[8] and alkene/CO_2 hydrogenation.[9] Unlike conventional heating, plasmon-driven catalysis handles hot electrons and/or a temperature gradient on the catalyst surface under light irradiation to accelerate the activity and shift the selectivity of reactions by activating specific chemical bonds. Amphiphilic plasmonic NPs (*e.g.*, HS-β-cyclodextrin modified with Ag NPs) can self-assemble at the water/oil interface giving improved signals for Surface-Enhanced Raman Spectroscopy (SERS) due to substrate activation by interfacial hot spots.[10] All and all, these studies clearly demonstrate the possibility of using plasmonic metal NPs as energy converters to drive catalytic reactions at moderate bulk temperature.

Herein, we developed a light-driven catalytic system based on a Pickering emulsion affording the oxidation of olefins at mild temperature. The system makes use of the colloidal tectonics approach to prepare emulsions, encompassing the interfacial self-assembly of two surface-active particles with complementary hydrophilic/hydrophobic groups (tectons).[11] The system combines silica NPs grafted with alkyl chains and Au NPs, acting as a heater/plasmon activator, and dodecyltrimethylammonium phosphotungstate NPs, $[C_{12}]_3[PW_{12}O_{40}]$, acting as the catalyst (Fig. 1).[12] The physicochemical pro-

[a]*Université de Lille, CNRS, Centrale Lille, Université Artois, UMR 8181 – UCCS – Unité de Catalyse et Chimie du Solide, F-59000 Lille, France. E-mail: veronique.rataj-nardello@univ-lille.fr*
[b]*Univ. Lille, CNRS, UMR 8523 – PhLAM – Physique des Lasers Atomes et Molécules, F-59000 Lille, France*
[c]*Univ. Lille, CNRS, UMR 8516 – LASIRe – Laboratoire Avancé de Spectroscopie pour les Intéractions la Réactivité et l'Environnement, F-59000 Lille, France*
[d]*Cardiff Catalysis Institute, School of Chemistry, Main Building, Cardiff University, Park Place, Cardiff CF10 3AT, UK. E-mail: peratitusm@cardiff.ac.uk*
† Electronic supplementary information (ESI) available. See DOI: https://doi.org/10.1039/d2gc04591e

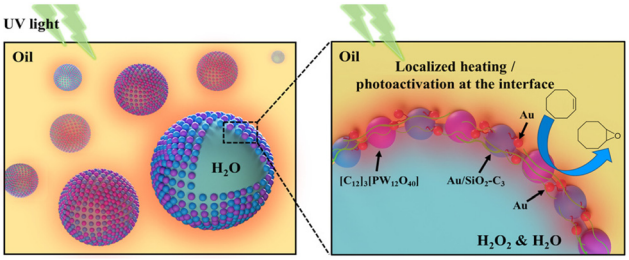

Fig. 1 Schematic representation of the emulsion system designed in this study using self-assembled amphiphilic silica NPs loaded with Au NPs, acting as on-site heater/plasmon activators, and $[C_{12}]_3[PW_{12}O_{40}]$ NPs, acting as the catalyst, under UV light irradiation.

perties, stability and interfacial plasmonic properties of the dual-NP stabilized emulsions were studied to assess the interaction between both NPs at the water/oil interface. The catalytic performance of the system was assessed for the oxidation of cyclooctene using H_2O_2 as the oxidant under UV light irradiation, and further extended to a panel of industrially relevant alkenes.

Results and discussion

Synthesis and characterization of particles

The hydrodynamic diameter and ζ-potential of the as-prepared NPs were measured by dynamic light scattering (DLS) (Table 1). In accordance with previous results,[12a] $[C_{12}]_3[PW_{12}O_{40}]$ NPs have a hydrodynamic diameter of 48 nm with a ζ-potential of −31.7 mV at pH 7. Au NPs have a hydrodynamic diameter of 13 nm with a ζ-potential of −34.7 mV. The hydrodynamic diameter of bare SiO_2 NPs is around 90 nm with a negative ζ-potential of −38 mV at pH 7. After surface modification, the ζ-potential of SiO_2–C_3 NPs becomes positive (+42.6 mV), which can be attributed to the protonation of amine groups on the silica surface. The hydrodynamic diameter of amphiphilic trimethoxy(propyl)- and aminopropyl-functionalized (SiO_2–C_3) NPs is about 200 nm, suggesting partial aggregation. The ζ-potential of SiO_2–C_3 NPs evolves from +59.9 mV to −49.4 mV on increasing the pH from 2 to 12 with the isoelectric point (IEP) at pH 10 (Fig. S1a†). After Au loading, Au/SiO_2–C_3 NPs exhibit a comparable hydrodynamic diameter (207 nm) and an analogous trend of the ζ-potential with pH, but the values are slightly lower than those of SiO_2–C_3 NPs (+40.3 *vs.* +42.6 mV at pH 7) (Fig. S1b†). This discrepancy suggests the presence of free amine groups after the decoration of SiO_2–C_3 with Au NPs. Increasing the Au loading in Au/SiO_2–C_3 from 8 to 24 μg (in 6 mL dispersion) results in a small decline of the ζ-potential. SiO_2–C_3 and Au/SiO_2–C_3 NP dispersions are stable below pH 8 and above 12, since the ζ-potential is outside the ±30 mV range.[13]

The surface morphology of dispersed Au, SiO_2–C_3 and Au/SiO_2–C_3 NPs was characterized by HR-TEM (Fig. 2). Dispersed Au NPs show a uniform spherical shape with an average size of 4.5 nm. This value is ≈3 times lower than the hydrodynamic diameter measured by DLS (13 nm, Table 1) which can be explained by the aggregation of Au NPs. SiO_2–C_3 NPs are also spherical with an average size of 26 nm and large size polydispersity, which is also lower than the hydrodynamic diameter (190 nm), suggesting aggregation of SiO_2–C_3 NPs. Au NPs on Au/SiO_2–C_3 (highlighted with red circles) are well dispersed and show an average size of 4.5 nm. The Au loading in Au/SiO_2–C_3 measured by ICP-OES is ≈0.13 wt%. The binding energy of the Au ($4f_{7/2}$) component for Au/SiO_2–C_3 measured by XPS is 83.9 eV (Fig. S2†), indicating that Au is mainly in its metallic state.[14]

Au NPs exhibit a neat surface plasmon resonance band in the UV spectrum at 518 nm (Fig. S3†), which matches earlier observations.[15] In the case of Au/SiO_2–C_3 NPs, the band slightly shifts to 528 nm, which can be explained by the shorter distance between Au NPs on Au/SiO_2–C_3 and by a change of the dielectric constant due to the silica environment.[15] Pure $[C_{12}]_3[PW_{12}O_{40}]$ NPs and a water solution of $H_3PW_{12}O_{40}$ do not show any UV absorption band.

The stability of the particles was studied by TGA. SiO_2 NPs show high thermal stability with a weight loss of 0.4% from 30 to 200 °C due to water desorption (Fig. S4†). A second weight loss is observed in the range of 200–900 °C which is attributed to the condensation of silanol groups. Both SiO_2–C_3 and Au/SiO_2–C_3

Table 1 Hydrodynamic diameter D_H and zeta potential ζ of NPs prepared in this study

	Au	SiO_2	SiO_2–C_3	Au/SiO_2–C_3	$[C_{12}]_3[PW_{12}O_{40}]$
D_H[a] (nm)	13	90	190	207	48
ζ[b] (mV)	−34.7	−38	42.6	40.3	−31.7

[a] Hydrodynamic diameter of NPs measured by DLS. [b] Determined for 0.1 wt% NP suspensions in water at 25 °C in neutral pH.

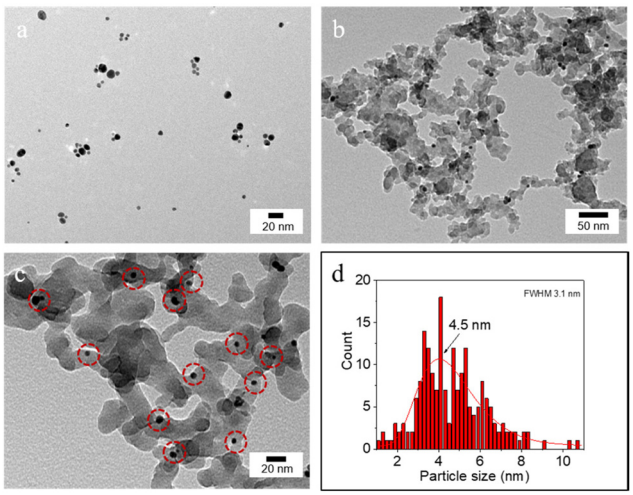

Fig. 2 HR-TEM micrograph of (a) Au NPs and (b and c) Au/SiO_2–C_3 NPs and (d) particle size distribution of Au NPs. The red circles in (c) indicate Au NPs immobilized on Au/SiO_2–C_3.

SiO_2–C_3 NPs show almost no weight loss (1.0 wt%) from 30 to 200 °C which is consistent with the hydrophobization of the samples. Both samples exhibit a weight loss of 15 wt% in the range of 400–600 °C which can be assigned to the decomposition of amine groups and C_3 chains, but with no significant weight loss in the range of 600–900 °C. These profiles illustrate the excellent stability of SiO_2–C_3 and Au/SiO_2–C_3 NPs.

To confirm the presence of grafted alkyl chains and amine groups on the silica surface, we recorded the FT-IR spectra of SiO_2, SiO_2–C_3 and Au/SiO_2–C_3 NPs (Fig. S5†). Two bands are visible at 1070 and 810 cm^{-1} for all samples which can be attributed to asymmetric and stretching vibrations of Si–O–Si bonds, respectively.[16] Characteristic bands appear at 2993/2904 cm^{-1} and 1505 cm^{-1} for SiO_2–C_3 and Au/SiO_2–C_3 NPs which can be ascribed to $-CH_2$ stretching vibrations in C_3 chains and bending vibrations of N–H groups,[17] respectively. Characteristic bands appearing at 930 cm^{-1} can be assigned to stretching modes of Si–C groups.[17] These results prove the grafting of SiO_2–C_3 and Au/SiO_2–C_3 NPs with $-C_3$ and $-NH_2$ chains.

The surface wettability of SiO_2, SiO_2–C_3 and Au/SiO_2–C_3 NPs was characterized by water contact angle analysis. SiO_2 NPs show no measurable contact angle because of instantaneous water absorption. In contrast, the water contact angle of SiO_2–C_3 is 108°, indicating that C_3 moieties successfully modify the silica surface (Fig. S6†). The contact angle for Au/SiO_2–C_3 NPs is slightly lower (98°), suggesting that the sample is slightly less hydrophobic. Finally, the contact angle of $[C_{12}]_3[PW_{12}O_{40}]$ NPs is about 93°. According to the Finkle rule,[18] emulsions stabilized with SiO_2–C_3 and Au/SiO_2–C_3 NPs are expected to be water-in-oil emulsions.

Physicochemical properties of Au/SiO_2–C_3/$[C_{12}]_3[PW_{12}O_{40}]$ NP stabilized Pickering emulsions

We studied the emulsification properties of combined Au/SiO_2–C_3 NPs + $[C_{12}]_3[PW_{12}O_{40}]$ NPs for a water/toluene (50 : 50 v/v) system as a function of the $[C_{12}]_3[PW_{12}O_{40}]$ weight fraction (Fig. 3). Both $[C_{12}]_3[PW_{12}O_{40}]$ and Au/SiO_2–C_3 NPs alone stabilize a water-in-toluene emulsion with an average droplet size of 18 μm and 22 μm, respectively. In the latter case, the emulsion becomes pink due to the presence of Au NPs. The combination of both NPs also generates a water-in-toluene emulsion, but the droplet size is much smaller (from 6 to 10 μm) than the values for both NPs alone. The combination of both NPs shows almost zero ζ-potential (−3 mV) at 0.2 wt%. Overall, these results confirm the remarkable synergy between both NPs at the water/oil interface.

We monitored the time-evolution of the emulsions stabilized with Au/SiO_2–C_3 NPs and $[C_{12}]_3[PW_{12}O_{40}]$ NPs alone and with combinations of both NPs (Fig. S7†). The combinations afford much more stable emulsions with no obvious collapse after 6 h at 60 °C. To gain more insight into the emulsion stability, light scattering measurements were performed using Turbiscan to monitor the change of transmission (ΔT) and backscattering (ΔBS) light intensity along the emulsion height (Fig. S8†). In the presence of $[C_{12}]_3[PW_{12}O_{40}]$ NPs, the emulsions

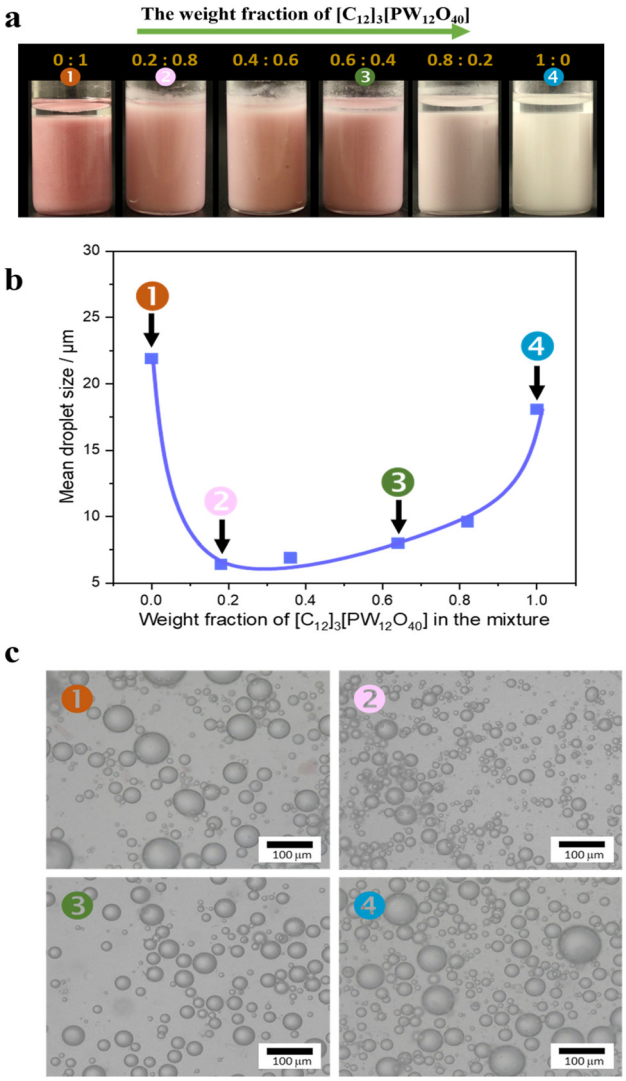

Fig. 3 (a) Images of emulsions stabilized with Au/SiO_2–C_3 NPs + $[C_{12}]_3[PW_{12}O_{40}]$ NPs at variable weight fractions; (b) evolution of the average droplet size against the $[C_{12}]_3[PW_{12}O_{40}]$ weight fraction for emulsions stabilized with Au/SiO_2–C_3 NPs + $[C_{12}]_3[PW_{12}O_{40}]$ NPs; (c) optical micrographs of water-in-oil emulsions. Emulsification conditions: 1.5 mL toluene, 1.5 mL water, 80 mg NPs (2.8 wt%), 11 500 rpm for 2 min.

exhibit a sharp decline of ΔBS in the top layer with a concomitant increase of the ΔT signal, which can be explained by clarification due to gravity-induced migration. Besides, ΔBS shows a slight decrease in the middle portion of the emulsion which can be interpreted as an increase in the droplet size due to either coalescence or flocculation. The ΔT signal remains almost unchanged over time, indicating no apparent stratification.

The emulsion is more stable when using combined Au/SiO_2–C_3 NPs + $[C_{12}]_3[PW_{12}O_{40}]$ NPs, as shown by the changes in the backscattering and transmission results. The slight change of ΔBS suggests lower creaming. On the top of the emulsion, the lower ΔBS and higher ΔT are in agreement with a clarified layer due to sedimentation and/or aggregation of droplets. The emulsion stability can be explained by the for-

mation of a compact interfacial layer of both NPs which likely protects the droplet surface and limits flocculation or coalescence of water droplets.[19]

With these results, we assessed the emulsion stability for Au/SiO_2–C_3 NPs + $[C_{12}]_3[PW_{12}O_{40}]$ NPs in the presence of cyclooctene and cyclooctene oxide (2 mol L^{-1}) (Fig. S9†). In both cases, the emulsion properties remain almost unchanged. However, in the latter case, the ΔBS signal is slightly lower within the tested height, but remains almost unchanged over time, suggesting neither creaming nor phase separation.

Study of plasmon-induced photothermal effects

We measured the photothermal curves of the Au NP dispersion and Au/SiO_2–C_3 NP-stabilized emulsion generated by light irradiation. The Au NP dispersion exhibits a marked increase of the bulk temperature (ΔT) of 24 °C *vs.* only 10 °C for pure water after 30 min (Fig. 4a). Increasing the amount of Au NPs from 4 to 40 μg (in 1 mL dispersion) leads to a ΔT increase from 16 to 24 °C with a maximal temperature of 48 °C at 40 μg Au. The Au/SiO_2–C_3 NP-stabilized emulsion displays a similar trend for 4 and 13 μg Au loading in the NPs (in 1 mL emulsion), with a ΔT of 20.6 °C and a maximal temperature of 47 °C at 13 μg Au after 30 min (Fig. 4b). However, no appreciable temperature change occurs upon further increasing the Au amount to 26 and 40 μg, encompassing a concomitant increase of the amount of Au/SiO_2–C_3 NPs in the system. This observation indicates a poorer heat transfer to the continuous phase at higher Au/SiO_2–C_3 NP loading, which can be attributed to two main reasons: (1) a high viscosity of the emulsion system that might hinder heat transfer from the water/toluene interface to the bulk phases[20] and (2) a denser packing of Au/SiO_2–C_3 NPs at the inner and outer interface of the droplets. As a result, the local temperature of the interfacial shell is expected to be much higher than the bulk temperature, with photon absorption.[21] The photothermal curves show a strong power-dependent effect for the Au NP dispersion and Au/SiO_2–C_3-stabilized emulsion upon increasing the power density from 260 to 1000 mW cm^{-2} (Fig. S10†).

Catalytic performance

Given the photothermal properties of the Au/SiO_2–C_3-stabilized emulsion, we aimed to effectively utilize light-induced interfacial heating/hot electrons to enhance the catalytic performance of $[C_{12}]_3[PW_{12}O_{40}]$ NPs. To this aim, we investigated the catalytic performance of combined Au/SiO_2–C_3 NPs + $[C_{12}]_3[PW_{12}O_{40}]$ NPs in the oxidation of cyclooctene. For comparison, control experiments were carried out under the same reaction conditions, but the reactor was heated in a thermostated bath to the same temperature reached in the tests under light. For instance, the temperature increases from 25 to 28 °C under light (260 mW cm^{-2}) for 60 min. Therefore, the bath temperature was set at 28 °C for the dark experiments. Preliminary tests were also conducted to optimize the reaction conditions (*i.e.* stirring rate, water/oil volume ratio, and weight of Au/SiO_2–C_3 and $[C_{12}]_3[PW_{12}O_{40}]$ NPs) (Fig. S11†). It has been previously demonstrated that 1.0 equiv. of H_2O_2 is needed to get 99% yield for the epoxidation of cyclohexene and cyclooctene in the Pickering emulsion systems.[12b] Since some H_2O_2 molecules are decomposed into H_2O and O_2 under light irradiation, the decomposition rate of H_2O_2 in the Pickering emulsion system (without the addition of the substrate) under light irradiation was measured by $KMnO_4$ titration.[22] The decomposition rate of H_2O_2 was 16% higher under light irradiation for 1 h than that without light irradiation. Therefore, 1.2 equiv. H_2O_2 were added for the epoxidation of cyclooctene.

No conversion is observed for blank experiments with Au/SiO_2–C_3 NPs under light and after heating to 28 °C (Fig. 4c). Using $[C_{12}]_3[PW_{12}O_{40}]$ NPs, the yield of cyclooctene oxide is about 19% with/without light at 95–100% selectivity, suggesting that light does not impact the catalytic properties. Combined $[C_{12}]_3[PW_{12}O_{40}]$ NPs and SiO_2–C_3 NPs exhibit a much

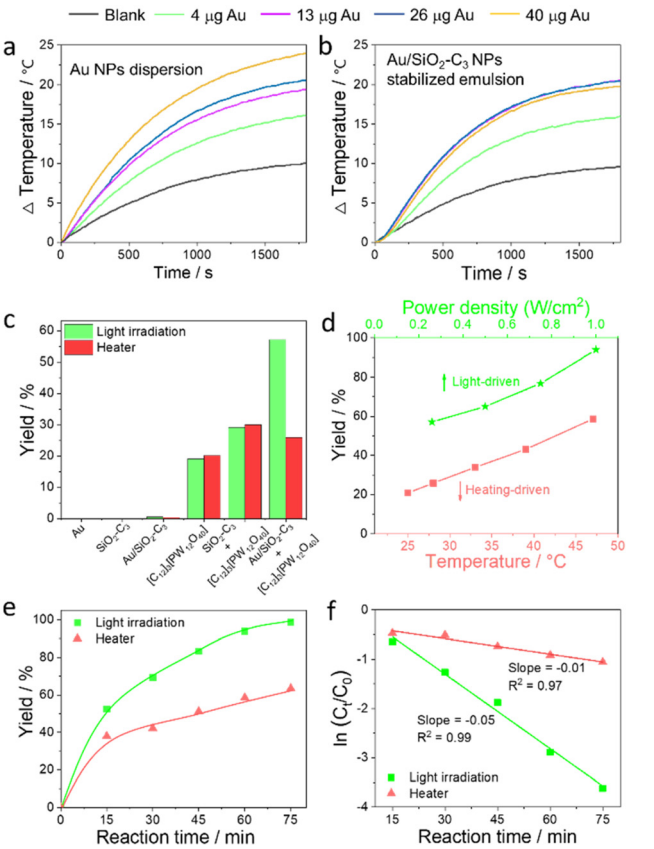

Fig. 4 Photothermal profiles of (a) Au NP dispersion and (b) Au/SiO_2–C_3-stabilized emulsion against Au loading (in 1 mL dispersion) at 1000 mW cm^{-2} power density for 30 min. (c) Yield of cyclooctene oxide (60 min) in cyclooctene oxidation over various NPs (*). (d) Yield of cyclooctene oxide (60 min) over $[C_{12}]_3[PW_{12}O_{40}]$ NPs + Au/SiO_2–C_3 NPs under light at variable power densities or after heating. (e and f) Time-evolution and kinetic plots of the yield of cyclooctene oxide over $[C_{12}]_3[PW_{12}O_{40}]$ + Au/SiO_2-C_3 NPs under light and heating. Reaction conditions: 30 mg Au/SiO_2–C_3 NPs, 50 mg $[C_{12}]_3[PW_{12}O_{40}]$ NPs, 1.5 mL toluene (2 mol L^{-1} cyclooctene), 1.5 mL water (containing 1.2 equiv. H_2O_2), emulsification at 11 500 rpm for 2 min, 120 rpm. Results based on ^1H NMR. (*) 40 μg Au NPs, 30 mg SiO_2–C_3 NPs, 30 mg Au/SiO_2–C_3 NPs, 50 mg $[C_{12}]_3[PW_{12}O_{40}]$ NPs, 50 mg $[C_{12}]_3[PW_{12}O_{40}]$ NPs + 30 mg SiO_2–C_3 NPs, 50 mg $[C_{12}]_3[PW_{12}O_{40}$, 260 mW cm^{-2}.

higher yield with/without light (30%) compared to that achieved for $[C_{12}]_3[PW_{12}O_{40}]$ NPs alone. This higher yield can be explained by the smaller droplet size and higher emulsion volume obtained when using combined SiO_2–C_3 NPs and $[C_{12}]_3[PW_{12}O_{40}]$ NPs owing to their synergy at the water/toluene interface (Fig. S12†). A catalytic test carried out with Au/SiO_2–C_3 NPs, but replacing $[C_{12}]_3[PW_{12}O_{40}]$ NPs with $H_3PW_{12}O_{40}$, which has no interfacial properties, shows only 8% yield of cyclooctene oxide after 60 min under light (1000 W cm^{-2}), whereas no conversion is observed for the tests performed either without light or in the absence of Au/SiO_2–C_3 NPs (Fig. S13†).

In contrast to these results, the reaction over combined Au/SiO_2–C_3 NPs and $[C_{12}]_3[PW_{12}O_{40}]$ NPs gives 57% yield of cyclooctene oxide after 60 min under light, whereas it decreases to 26% at 28 °C. The yield increases linearly from 57% to 94% with the increase of power density (range 260–1000 mW cm^{-2}) (Fig. 4d), but only an increase from 27% to 45% was achieved for the tests in a thermostated bath with the same temperature increase (from 28 to 47 °C after 60 min). The yield of cyclooctene oxide is almost 100% after 75 min under light (1000 mW cm^{-2}), but it is only 63% at 47 °C (Fig. 4e).

Cyclooctene oxidation follows an apparent first-order kinetics (Fig. 4f) with a kinetic constant of k = 0.05 min^{-1} under light (1000 mW cm^{-2}), which is much larger than k = 0.01 min^{-1} at 47 °C. In parallel, the turnover frequency (TOF) is 188 h^{-1} under light, whereas it is 88 h^{-1} when using $[C_{12}]_3[PW_{12}O_{40}]$ NPs alone. Additional catalytic tests conducted using a 532 nm pulsed laser (100 mW cm^{-2}), with higher photonic efficiency, deeper penetration and sharper spectrum than UV lamps, afforded 91% yield of cyclooctene oxide after 60 min despite the lower power density, while it is much lower (50%) at 43 °C corresponding to the temperature reached during the laser-driven catalytic reaction (Fig. S14†).

Overall, this body of results outline the enhanced catalytic efficiency of combined Au/SiO_2–C_3 NPs and $[C_{12}]_3[PW_{12}O_{40}]$ NPs for cyclooctene oxidation. Such a promoting effect can be ascribed to three factors: (1) preferential location of catalytic sites (*i.e.* $[C_{12}]_3[PW_{12}O_{40}]$) at the water/toluene interface leading to greater contact with cyclooctene and favouring mass transfer; (2) synergy between both NPs allowing plasmon-driven heating/activation under light; and (3) coverage of the droplet surface by a thick layer of closely packed NPs allowing high emulsion stability and hindering heat transfer to the bulk phases.

Catalyst recyclability and reuse

The recyclability and reuse of Au/SiO_2–C_3 and $[C_{12}]_3[PW_{12}O_{40}]$ NPs were studied for cyclooctene oxidation over five consecutive catalytic cycles. After each cycle, the reaction medium was centrifuged (5000 rpm, 30 min), and the particles were separated and dried at 80 °C for 12 h before use in the subsequent cycle. The particles can be conveniently recycled after each run without apparent loss of catalytic activity and emulsification properties (Fig. 5). This body of results evidence the absence of significant catalyst deactivation during the reaction. The HR-TEM micrographs of the recovered Au/SiO_2–C_3 NPs and $[C_{12}]_3[PW_{12}O_{40}]$ NPs after the fifth cycle show no change in the size distribution of Au NPs over Au/SiO_2–C_3 compared to the fresh sample with an average size of 4.2 nm. However, partial agglomeration of Au NPs is observed (Fig. S15†). $[C_{12}]_3[PW_{12}O_{40}]$ NPs are deposited on Au/SiO_2–C_3 NPs (not shown), confirming their interaction. On the other hand, it should also be mentioned that W-based catalysts can be prone to metal leaching. Indeed, while some studies have demonstrated that leached W species cannot act as a catalyst by themselves,[23] Bisio *et al.* have shown that in the presence of hydrogen peroxide, they themselves can act as a catalyst for alkene epoxidation.[23] So, a study of tungsten leaching in the system stabilized with Au/SiO_2–C_3 and $[C_{12}]_3[PW_{12}O_{40}]$ NPs could be useful to confirm the impact of the nature of the polyoxometalates on different substrates.

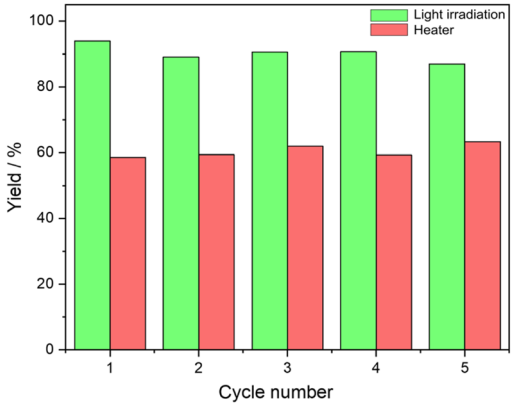

Fig. 5 Recyclability and reuse of Au/SiO_2–C_3 and $[C_{12}]_3[PW_{12}O_{40}]$ NPs (40/60 wt%) for cyclooctene oxidation over five consecutive cycles. Reaction conditions: 30 mg Au/SiO_2–C_3 NPs, 50 mg $[C_{12}]_3[PW_{12}O_{40}]$ NPs, 1.5 mL toluene (2 mol L^{-1} cyclooctene), 1.5 mL water (containing 1.2 equiv. of H_2O_2), emulsification at 11 500 rpm for 2 min, 120 rpm. Results based on ^1H NMR.

Scope of reactants

To assess the versatility of combined $[C_{12}]_3[PW_{12}O_{40}]$ NPs and Au/SiO_2–C_3 NPs in emulsion for light-driven oxidation reactions, we tested cyclohexene, limonene and 1-octene, and compared the results obtained after heating to 47 °C which corresponds to the temperature reached under light (Table 2). Cyclohexene oxidation results mainly in 1,2-cyclohexanediol with 70% yield after 1 h under light irradiation (entry 2). In contrast, the yield is 57% at 47 °C. In both cases, no cyclohexene epoxide is observed due to fast ring opening in emulsion, matching the results of a previous study.[11c] In the case of limonene with two unsaturations, the epoxidation of the exocyclic unsaturation is achieved as a secondary reaction of the epoxidation of the endocyclic unsaturation. It is still challenging to get 8,9-limonene oxide or limonene dioxide, and 1,2-limonene oxide is obtained as the main product together with carvone as the minor product.[24] Although limonene conversion is slightly lower under light than in the experiment at 47 °C (35% *vs.* 45% after 2 h), the yield of 1,2-limonene oxide is higher in the former case (29% *vs.* 11%) due to a much higher selectivity

Table 2 Catalytic results for the oxidation of olefins in a water/toluene emulsion stabilized with Au/SiO_2–C_3 + $[C_{12}]_3[PW_{12}O_{40}]$ NPs

		Light irradiation		Heater (47 °C)	
Substrate	t/h	Conv. (%)	Yield (%)	Conv. (%)	Yield (%)
	1	94	94[a]	61	58[a]
	1	70	70[b]	57	57[b]
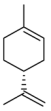	2	35	29[c]/8[d]	45	11[c]/7[d]
	2	12	11[e]	3	3[e]

Reaction conditions: 30 mg Au/SiO_2–C_3 NPs, 50 mg $[C_{12}]_3[PW_{12}O_{40}]$ NPs, 1.5 mL toluene (containing 2 mol L^{-1} substrates) and 1.5 mL water (containing 1.2 equiv. of H_2O_2), emulsification at 11 500 rpm for 2 min, 60 min, 120 rpm. [a] Results based on ^{1}H NMR of cyclooctene oxide. [b] Results based on ^{1}H NMR of 1,2-cyclohexanediol. [c] Results based on ^{1}H NMR of 1,2-limonene oxide. [d] Results based on ^{1}H NMR of carvone. [e] Results based on ^{1}H NMR of 1,2-epoxyoctane.

(83% *vs.* 24%). The oxidation of 1-octene shows 11% yield of 1,2-epoxyoctane after 2 h in the light-driven test, whereas only 3% yield is obtained at 47 °C. Overall, these results demonstrate the ability of combined Au/SiO_2–C_3 and $[C_{12}]_3[PW_{12}O_{40}]$ NPs for the light-driven oxidation of olefins at the water/toluene interface.

Photo- *vs.* thermal reactor: energy savings

Reduction of energy consumption is key to developing more eco-efficient processes. In this section, we aim to assess if plasmon-driven interfacial heating/activation under light irradiation could provide energy savings for biphasic reactions in emulsion compared to conventional thermal heating. In this view, by using the above body of results, we estimated the energy required in the light-driven and control experiments in our labscale reactor.

The determination of the theoretical energy (Q_{TH}) that is required for a reaction mixture to reach a given temperature (heating + cooling) can be calculated using eqn (1), whereas the energy input supplied by the lamp (Q_L) can be computed using eqn (2) which depends on the power dissipation and time of exposure. From eqn (1) and (2), the overall energy saving factor (η) of light irradiation compared to the energy required in thermal experiments can be calculated using eqn (3)

$$Q_{TH} = 2\sum_{\alpha} m_{\alpha} C_{p,\alpha} \Delta T \quad (1)$$

$$Q_L = P_{avg} \Delta T \quad (2)$$

$$\eta = \left(\frac{Q_{TH} - Q_L}{Q_{TH}}\right) \quad (3)$$

where m_α is the mass of each phase in the biphasic system (g); $C_{p,\alpha}$ is the specific heat capacity of each phase (J g^{-1} °C^{-1}); ΔT is the temperature change observed for the reaction (°C), P_{avg} is the average power output of the lamp (W) and ΔT is the light irradiation time (h).

For a 10 mL water/toluene emulsion (50 : 50 v/v) in a lab scale batch reactor and cyclooctene oxidation for 1 h under light irradiation (260 mW cm^{-2} UV lamp) and thermal heating (47 °C), a similar cyclooctene yield (58%) is obtained, and the energy factor is about 74% (see detailed calculations in the ESI†). This result outlines the energy benefits of photoreactors based on particle-stabilised emulsions compared to standard thermal reactors for conducting oxidation reactions.

Conclusions

In summary, we have designed a novel emulsion system that combines interfacial heating/activation by plasmonic Au/SiO_2–C_3 NPs under light irradiation and the catalytic properties of $[C_{12}]_3[PW_{12}O_{40}]$ NPs for near-room temperature oxidation of alkenes with H_2O_2. The dual-NP system exhibits a 5-fold increase of activity compared to the thermal reaction, and can be recycled and reused for at least five consecutive catalytic runs. The enhanced catalytic properties are ascribed to the intimate contact between both NPs at the water/toluene interface, discouraging heat transfer to the bulk phase. The concept presented in this study, although in its infancy, opens an avenue for engineering multiphase catalytic photoreactors with a potential energy saving of 74% at isoconversion compared to conventional thermal reactors. Further investigations will be conducted with a special emphasis on the effect of the wavelength of light irradiation on the system.

Author contributions

YF: investigation, methodology, visualization, and writing – original draft; JFD: conceptualization, supervision, validation, and writing – review & editing; QA: investigation and writing – review & editing; EC: resources and writing – review & editing; VD: resources and writing – review & editing; MPT: conceptualization, validation, and writing – review & editing; VNR: conceptualization, acquisition, resources, supervision, validation, visualization, and writing – review & editing.

Conflicts of interest

There are no conflicts to declare.

Acknowledgements

This work was funded by the Chevreul Institute (FR2638), Ministère de l'Enseignement et de la Recherche, Région Hauts de France and FEDER. Financial support from China Scholarship Council is also acknowledged. The authors would also like to thank Jean Pesez for his help in pulsed laser experiments and fruitful discussions.

References

1 (*a*) L. Wang, M. Hasanzadeh Kafshgari and M. Meunier, *Adv. Funct. Mater.*, 2020, **30**, 2005400; (*b*) J. Liu, H. He, D. Xiao, S. Yin, W. Ji, S. Jiang, D. Luo, B. Wang and Y. Liu, *Materials*, 2018, **11**, 1833; (*c*) A. Sanchot, G. Baffou, R. Marty, A. Arbouet, R. Quidant, C. Girard and E. Dujardin, *ACS Nano*, 2012, **6**, 3434.

2 (*a*) M. Hu, J. Chen, Z.-Y. Li, L. Au, G. V. Hartland, X. Li, M. Marquez and Y. Xia, *Chem. Soc. Rev.*, 2006, **35**, 1084; (*b*) P. K. Jain, X. Huang, I. H. El-Sayed and M. A. El-Sayed, *Plasmonics*, 2007, **2**, 107; (*c*) X. Huang, P. K. Jain, I. H. El-Sayed and M. A. El-Sayed, *Lasers Med. Sci.*, 2008, **23**, 217; (*d*) M. A. Mackey, M. R. K. Ali, L. A. Austin, R. D. Near and M. A. El-Sayed, *J. Phys. Chem. B*, 2014, **118**, 1319; (*e*) H. Liu, D. Chen, L. Li, T. Liu, L. Tan, X. Wu and F. Tang, *Angew. Chem., Int. Ed.*, 2011, **50**, 891; (*f*) M. Sharifi, F. Attar, A. A. Saboury, K. Akhtari, N. Hooshmand, A. Hasan, M. A. El-Sayed and M. Falahati, *J. Controlled Release*, 2019, **311**, 170.

3 (*a*) K. Jiang, D. A. Smith and A. Pinchuk, *J. Phys. Chem. C*, 2013, **117**, 27073; (*b*) J. Qiu and W. D. Wei, *J. Phys. Chem. C*, 2014, **118**, 20735; (*c*) J. Zheng, X. Cheng, H. Zhang, X. Bai, R. Ai, L. Shao and J. Wang, *Chem. Rev.*, 2021, **121**, 13342.

4 (*a*) R. Ma, J. Sun, D. H. Li and J. J. Wei, *Int. J. Hydrogen Energy*, 2020, **45**, 30288; (*b*) S. Luo, X. Ren, H. Lin, H. Song and J. Ye, *Chem. Sci.*, 2021, **12**, 5701; (*c*) D. Mateo, J. L. Cerrillo, S. Durini and J. Gascon, *Chem. Soc. Rev.*, 2021, **50**, 2173.

5 C. Fasciani, C. J. B. Alejo, M. Grenier, J. C. Netto-Ferreira and J. C. Scaiano, *Org. Lett.*, 2011, **13**, 204.

6 (*a*) X. Huang, Y. Li, Y. Chen, H. Zhou, X. Duan and Y. Huang, *Angew. Chem., Int. Ed.*, 2013, **52**, 6063.

7 A. Pineda, L. Gomez, A. M. Balu, V. Sebastian, M. Ojeda, M. Arruebo, A. A. Romero, J. Santamaria and R. Luque, *Green Chem.*, 2013, **15**, 2043.

8 (*a*) G. Liu, Q. Xiong, Y. Xu, Q. Fang, K. C.-F. Leung, M. Sang, S. Xuan and L. Hao, *Colloids Surf., A*, 2022, **633**, 127860; (*b*) Y. Zhao, R. M. Sarhan, A. Eljarrat, Z. Kochovski, C. Koch, B. Schmidt, W. Koopman and Y. Lu, *ACS Appl. Mater. Interfaces*, 2022, **14**, 17259.

9 (*a*) L. C. de la Garza, N. Brodusch, R. Gauvin and A. Moores, *ACS Appl. Nano Mater.*, 2021, **4**, 1596; (*b*) Z. Tang, F. Zhu, J. Zhou, W. Chen, K. Wang, M. Liu, N. Wang and N. Li, *Appl. Catal., B*, 2022, **309**, 121267.

10 L. Ouyang, D. Li, L. Zhu, W.-W. Yang and H. Tang, *J. Mater. Chem. C*, 2016, **4**, 736.

11 (*a*) L. Leclercq, *Front. Chem.*, 2018, **6**, 168; (*b*) B. Yang, L. Leclercq, V. Schmitt, M. Pera-Titus and V. Nardello-Rataj, *Chem. Sci.*, 2019, **10**, 501; (*c*) B. Yang, G. Douyère, L. Leclercq, V. Nardello-Rataj and M. Pera-Titus, *Catal. Sci. Technol.*, 2020, **10**, 6723.

12 (*a*) L. Leclercq, A. Mouret, S. Renaudineau, V. Schmitt, A. Proust and V. Nardello-Rataj, *J. Phys. Chem. B*, 2015, **119**, 6326; (*b*) L. Leclercq, A. Mouret, A. Proust, V. Schmitt, P. Bauduin, J.-M. Aubry and V. Nardello-Rataj, *Chem. – Eur. J.*, 2012, **18**, 14352.

13 G. Douyère, L. Leclercq and V. Nardello-Rataj, *Colloids Surf., A*, 2021, **631**, 127705.

14 C. Oliveira, C. Ribeiro Chaves, P. Bargiela, M. da Graça Carneiro da Rocha, A. Ferreira da Silva, J. F. Diniz Chubaci, M. Boström, C. Persson and M. Malta, *J. Mater. Res. Technol.*, 2021, **15**, 768.

15 (*a*) S. M. Demers, C. R. Shirazinejad, J. L. A. Garcia, J. R. Matthews and J. H. Hafner, *J. Phys. Chem. C*, 2017, **121**, 5201; (*b*) S. S. Shankar, S. Bhargava and M. Sastry, *J. Nanosci. Nanotechnol.*, 2005, **5**, 1721; (*c*) M. Santana Vega, F. Brisset and G. Laurent, *Plasmonics*, 2021, **16**, 635.

16 G. D. Chukin and V. I. Malevich, *J. Appl. Spectrosc.*, 1977, **26**, 223.

17 (*a*) D. Lin-Vien, W. G. Fateley, N. B. Coltup and J. G. Grasselli, *The Handbook of Infrared and Raman Characteristic Frequencies of Organic Molecules*, Academic Press, 1991; (*b*) B. Yang, L. Leclercq, J.-M. Clacens and V. Nardello-Rataj, *Green Chem.*, 2017, **19**, 4552.

18 P. Finkle;, H. D. Draper; and J. H. Hildebrand, *J. Am. Chem. Soc.*, 1923, **45**, 2780.

19 S. Arditty, C. P. Whitby, B. P. Binks, V. Schmitt and F. Leal-Calderon, *Eur. Phys. J. E*, 2003, **11**, 273.

20 (*a*) F. Wang, W. Lin, Z. Ling and X. Fang, *Sol. Energy Mater. Sol. Cells*, 2019, **191**, 218; (*b*) R. Bielas, T. Hornowski, K. Paulovičová, M. Rajňák and A. Józefczak, *J. Mol. Liq.*, 2020, **320**, 114388; (*c*) R. Bielas and A. Józefczak, *Materials*, 2020, **13**, 4783.

21 (*a*) C.-H. Chou, C.-D. Chen and C. C. Wang, *J. Phys. Chem. B*, 2005, **109**, 11135; (*b*) L. François, M. Mostafavi, J. Belloni, J.-F. Delouis, J. Delaire and P. Feneyrou, *J. Phys. Chem. B*, 2000, **104**, 6133; (*c*) M. Bryckaert, A. Kharchenko, O. Lebedev, B. Dong, I. De Waele, G. Buntinx, O. Poizat, S. Mintova and V. De Waele, *J. Phys. Chem. C*, 2017, **121**, 26958.

22 C. E. Huckaba and F. G. Keyes, *J. Am. Chem. Soc.*, 1948, **70**, 1640.

23 (*a*) N. Mizuno, K. Yamaguchi and K. Kamata, *Catal. Surv. Asia*, 2011, **15**, 68; (*b*) N. Maksimchuk, I. Ivanchikova, O. Zalomaeva, Y. Chesalov, A. Shmakov, V. Zaikovskii and O. Kholdeeva, *Catalysts*, 2018, **8**, 95; (*c*) C. Bisio, A. Gallo, R. Psaro, C. Tiozzo, M. Guidotti and F. Carniato, *Appl. Catal., A*, 2019, **581**, 133.

24 (*a*) S. G. Casuscelli, M. E. Crivello, C. F. Perez, G. Ghione, E. R. Herrero, L. R. Pizzio, P. G. Vazquez, C. V. Caceres and M. N. Blanco, *Appl. Catal., A*, 2004, **274**, 115; (*b*) Y. M. Ahmat and S. Kaliaguine, *Catal. Today*, 2023, **407**, 146.